Influence of polarization effects and magnetic fields on time-resolved laser-induced fluorescence measurements

W. Schade
Institut für Experimentalphysik, Universität Kiel, Olshausenstraße 40, D-2300 Kiel, Germany

L. Wolejko
Institute of Physics, A. Mickiewicz University, Poznan, Poland

V. Helbig
Institut für Experimentalphysik, Universität Kiel, Olshausenstaße 40, D-2300 Kiel, Germany
(Received 3 August 1990; revised manuscript received 8 September 1992)

The theory of time-resolved laser-induced fluorescence (LIF) in a static magnetic field is reformulated by means of the graphical method of angular momentum theory. Invariant general geometrical relations of the time-resolved fluoresence signal are obtained in an explicit form for arbitrary polarization and propagation directions of the primary and secondary radiation and for any direction of the magnetic field. On this basis an extensive experimental study was carried out to find general conditions for lifetime experiments using laser-induced fluorescence, under which the direction of polarization in the excitation and the observation channel and the influence of external magnetic fields does not change the time evolution of the fluorescence signal. It is shown that besides the well-known "magic-angle" excitation also measurements at very low pressures ($p \approx 10^{-4}$ mbar) provide conditions where laser-induced alignment is negligible and does not disturb the time evolution of the decay signal. Furthermore the experiments confirm that the magnitude of laser-induced alignment depends very sensitively on the chosen transition scheme, on the value of the cross section for alignment destroying collisions, and on the geometry of the experiment. Interferences on the time-resolved fluorescence signal by external magnetic fields are also discussed. It is shown that the presence of a strong magnetic field can lead to lifetime results systematically too short under conditions typical for LIF lifetime experiments.

PACS number(s): 32.60.+i, 32.70.Fw, 32.50.+d

I. INTRODUCTION

Accurate absolute oscillator strengths of atomic and ionic transitions are of great interest in the astrophysical analysis of stellar spectra, in the diagnostics of impurities of fusion plasmas and in the understanding of technical discharge plasmas. There are two methods to measure absolute oscillator strengths. One is to use the emission of plasmas close to or in thermodynamic equilibrium. Either the electron density or the temperature is then determined by spectroscopic plasma diagnostics. The accuracy for the atomic data derived from such experiments is typically 25%.

The other, more reliable method of determining absolute oscillator strengths is the combination of precise lifetime values with the results of branching-ratio measurements. The absolute uncertainty of branching ratios from emission experiments is typically 2%–5% when the detection system is carefully calibrated, intensity loss in the far line wings of the spectral lines is taken into account and it is verified that the emitting plasma is optical thin. The uncertainty of the data derived from a lifetime experiment is typically about 5%. The combination of these lifetimes with the branching ratios from emission experiments yields absolute oscillator strengths with an accuracy between 3% and 7%.

Wiese *et al.* [1] have recently performed a compilation of atomic transition probabilities for neutral argon to present a unified set of these data. Argon has long been considered a test case to study the various diagnostic techniques. The numerous experimental and theoretical papers have been reviewed in detail by Wiese [2,3]. In Ref. [1] the absolute scale has been derived by a combination of radiative lifetimes with branching ratios from emission experiments. Radiative lifetimes of neutral argon have been the subject of quite a few investigations in the past. As an example, the lifetime results of the $3p$ levels (Paschen notation) from the various authors differ by as much as a factor of 3. This is surprising in so far as measuring lifetimes in the range of 100 ns and observing the emitted fluorescence in the blue region of the spectrum should not cause any experimental difficulties. Recent measurements in our laboratory concerning the lifetime of the $3p_8$ level of neutral argon have pointed out this problem [4].

Among various methods of determining the lifetimes of excited atomic and ionic levels [5], time-resolved laser-induced fluorescence (TRLIF) is distinguished by its very basic physical interpretation [6–8]. Progress in the technology of tunable pulsed lasers and in recording techniques has caused that this method has recently become very versatile and reliable. In particular, the application of the single-photon-counting technique [9–11] has ensured linearity of detection over a wide dynamic range

and has made it possible to achieve high accuracy in atomic and ionic lifetime measurements [12,13].

However, a number of systematic errors may prevent the observation of the undisturbed lifetime from the time-resolved fluorescence signal. Some are related to the method itself, as there are the finite width of the excitation pulse, pileup, flight-out-of-view, polarization effects in the excitation and in the observation channel and external magnetic fields, while others are connected to the phenomena investigated, as radiation trapping and collisional effects [4,6–8].

In high accuracy TRLIF experiments special attention should be given to all of these effects. However, in most lifetime experiments performed so far only one or two of them have been explicitly taken into account. The influence of the direction of polarization of the exciting laser radiation and influences on the time-resolved fluorescence signal resulting from residual magnetic fields usually have been neglected completely. This is astonishing in so far as Hannaford and Lowe [8] have given in 1983 a quantitative theoretical description of these phenomena and Fujimoto, Goto, and Fukuda [14,15] already in 1981 have pointed out that the laser-induced alignment of the upper-level population can disturb the observation of the fluorescence signal. Nevertheless, up to now no complete theoretical and experimental summary of these phenomena with regard to systematic errors in lifetime experiments exists in the literature.

The leading idea of this paper is to show under which experimental conditions in TRLIF measurements polarization effects and external magnetic fields will significantly disturb the time evolution of the fluorescence signal and under which conditions not.

For that reason the theory of TRLIF is reformulated applying graphical methods of the quantum theory of angular momentum [16–22]. The analysis is performed throughout with that formalism and almost all the analytical results are simply transliterations of their own diagrammatic counterparts. This approach, together with the use of the density-matrix technique [23,24], allows us to obtain general geometrical relations in compact and invariant form for arbitrary polarization and propagation directions of the primary and secondary radiation and for any direction of the magnetic field. The formulas are easily applicable to any geometry of the TRLIF experiment and have been used to calculate synthetic fluorescence signals to find out the best experimental conditions to observe or to prevent polarization and magnetic field effects of the measured decay signals. The calculated and the measured fluorescence signals have then been compared and in all investigated cases very good agreement between theory and experiment is observed.

It follows from the theoretical calculations that the largest contribution of the laser-induced alignment term is expected in the first part of the time-resolved fluorescence signal. Therefore much care has been taken to avoid any influence of the finite pulse width of the exciting laser pulse on the measured decay curves. In this experiment the states under investigation were selectively excited by a pulsed dye laser system which produces tunable subnanosecond pulses with a repetition rate of up to 200 Hz [11,25,26]. Influences of the finite pulse duration on the measured decay curves are then negligible [11].

The atoms and ions were produced in a pulsed low-pressure hollow cathode and the fluorescence signal was detected with a standard photon-counting system [11,27]. The pressure in the excitation volume was varied from 10^{-4} to 10 mbar and the field strength of the external magnetic field was varied from 0 to 95 G. Objects of this investigation have been the neon I $3p'[1/2]_1$ and the argon I $5p[5/2]_2$ states.

II. THEORETICAL BACKGROUND

It is our intention to determine general geometrical relations for TRLIF signals in the presence of a static magnetic field in simple vectorial form. To this end we take advantage of the graphical techniques of the angular momentum theory of Jucys, Levinson, and Vanagas [16–22] and we refer to the appropriate graphs as JLV diagrams [17,21].

The crucial feature of our approach is the application of the angular momentum coupling trees reduction methods elaborated by Stedman [21]. They allow us to express the final results in terms of the minimal set of rotationally invariant parameters, like scalar and triple products of the vectors involved. These invariants are also free of the base choice. Thus, one can interpret results in Cartesian rather than in spherical coordinates.

The graphical approach presents the exactness and other well-known advantages of the analytic method like separability of the physical processes into geometrical factors and atomic constants on the basis of the Wigner-Eckart theorem [21], on the one hand, and ensures the optimal computational efficiency and transparency, on the other.

In this presentation an atomic system under the action of a laser pulse in the presence of a constant magnetic field $\mathbf{B}$ is considered. Hyperfine-structure quantum beats are not involved. It is assumed that the mean value of the exciting laser light wavelength λ_L corresponds to transitions between unperturbed multiplets $\{g\}$ and $\{s\}$, whereas the bandwidth of the pulse is broad enough to cover the whole spectral range of these transitions broadened by the simultaneous interaction of the atom with the magnetic field, the radiation field, and other atoms (broadband excitation). Further on the energy density $u(\tau)$ of the laser pulse at the moment τ is assumed to be constant within the spectral region of optical transitions between the two manifolds. We also neglect the effect of radiation trapping, saturation, stimulated emission, and the initial state is assumed to be isotropic (no self-alignment).

The fundamental quantity in TRLIF is the time-dependent signal of the fluorescence $S(t)$ measured as the photodetector counting rate. This signal is assumed to be proportional to the intensity of the fluorescence light on traversing a filtering device which selects the quasiplane mode with given propagation direction $\mathbf{k}_D$, polarization vector $\boldsymbol{\epsilon}$, and wavelength λ_D from the spherical waves emitted by the atoms. The signals thus defined can be

treated as an expectation value of a detection operator $D(\epsilon)$ for the fluorescence [6–8,24,28]

$$S(t)=\mathrm{Tr}[\rho(t)D(\epsilon)] , \tag{1}$$

where $\rho(t)$ is a density matrix of an atomic system at a time t. We assume the density matrix to be independent of the position and velocity of the atoms.

In the electric dipole approximation the detection operator, comprising also functions of the filtering device, has the form

$$D(\epsilon)=C_D \sum_{f,s,s'} |s'\rangle\langle s'|\mathbf{d}\cdot\epsilon|f\rangle\langle f|\mathbf{d}\cdot\epsilon^*|s\rangle\langle s| , \tag{2}$$

where $\mathbf{d}$ is the electric dipole-moment operator of the atom, and ϵ is in general a complex vector with the conjugated counterpart ϵ^*. The constant C_D which contains well-known parameters of the electron dipole radiation as well as other coefficients not essential for our considerations will be dropped in further steps. These coefficients comprise the sensitivity of the detection system which we assume to be constant in the spectral range of recording.

The states $|s\rangle$ and $|s'\rangle$ belong to the set $\{s\}$ from which the detected fluorescence starts, whereas the states $|f\rangle$ belong to the $\{f\}$ manifold, where it ends. We can select groups of initial and final states by proper setting of the transmission bandwidth of the monochromator. Thus, summation in Eq. (2) covers products of all interfering transitions undistinguishable by the filter. In the case under consideration the manifolds $\{s\}$ and $\{f\}$ represent two different Zeeman multiplets.

We perform our calculations in the orthogonal basis of stationary atomic states $|a\rangle=|n_a,a,\alpha\rangle$ which are angular momentum eigenvectors with the total angular momentum given by the quantum number a, and its projection on the quantization axis labeled by α; n_a stands for the remaining indices necessary to specify the state; the latter will be omitted in our further notation. We use the primed symbol to distinguish states with the same value of the total angular momentum $a=a'$ (also $n_a=n_a'$), that have to be summed independently over the magnetic quantum numbers.

In the basis assumed Eq. (1) reads

$$S(t)=\sum_{a,\alpha,a',\alpha'} \langle a\alpha|\rho(t)|a'\alpha'\rangle\langle a'\alpha'|D(\epsilon)|a\alpha\rangle . \tag{3}$$

In terms of the JLV diagrams this equations is

$$S(t) = \sum_{a,a'} \left(\rho\right)_{a'}^{a} \left(D\right) , \tag{3'}$$

which serves as starting point for our graphical analysis of the TRLIF signal.

This calculation is shown in detail in Appendix A and leads for the TRLIF signal to the final equation (A21):

$$S(t)\propto \sum_k \alpha(k)\exp(-\Gamma_k t)F_k(t) , \tag{4}$$

with the anisotropy factor $\alpha(k)$, the decay rate of the kth multipole moment Γ_k and the general time-dependent geometrical factor $F_k(t)$ given by Eqs. (A19) and (A20). The latter one represents the angular distribution function for the population ($k=0$), orientation ($k=1$), and alignment ($k=2$) term in the TRLIF signal of Eq. (4).

According to the results of Stedman [21] we can express the angular momentum coupling trees of $F_k(t)$ as combinations of invariant products of the vectors involved:

$$F_0(t)=\tfrac{1}{3} , \tag{5a}$$

$$F_1(t)=-\tfrac{1}{2}(\epsilon\times\epsilon^*)\cdot[\mathbf{e}(t)\times\mathbf{e}(t)^*] , \tag{5b}$$

$$F_2(t)=\tfrac{1}{6}[3|\epsilon\cdot\mathbf{e}(t)^*|^2+3|\epsilon\cdot\mathbf{e}(t)|^2-2] . \tag{5c}$$

The vectors $\mathbf{e}$ and ϵ are the polarization vectors in the excitation and observation channel and $\mathbf{e}^*$ and ϵ^* are the conjugated counterparts. Due to the Eq. (A17) the factors (5b) and (5c) can be written in terms of time-independent vectors. Performing elementary vectorial calculations we get for the function of the angular distribution of the orientation signal the following expression:

$$F_1(t)=\tfrac{1}{2}(\eta_L\eta_D)[(\mathbf{k}_L\cdot\mathbf{k}_D)\cos\Omega t+(\mathbf{k}_L\cdot\mathbf{b})(\mathbf{k}_D\cdot\mathbf{b})(1-\cos\Omega t)+\mathbf{b}\cdot(\mathbf{k}_L\times\mathbf{k}_D)\sin\Omega t] , \tag{6}$$

where we have used the relations [21]

$$\mathbf{e}\times\mathbf{e}^*=-i\mathbf{k}_L\eta_L, \quad \epsilon\times\epsilon^*=-i\mathbf{k}_D\eta_D . \tag{7}$$

η_L (and η_D) is the Stokes parameter (S_3 in Born and Wolf [29] notation) related to the ellipticity of the exciting (and the detected) light, $\mathbf{k}_L$ and $\mathbf{k}_D$ point in the direction of light propagation in the excitation and observation channels, and $\mathbf{b}$ is the unit vector parallel to the magnetic field. It results from Eqs. (6) and (7) that the application of a linear polarizer in one channel only, either in excitation ($\eta_L=0$) or in detection ($\eta_D=0$), eliminates completely the contribution of orientation from the total TRLIF signal.

The angular distribution function of the alignment signal $F_2(t)$ has, in the general case, a much more complex form but can always be expressed as the following series:

$$F_2(t)=a_0+a_1\cos\Omega t+a_2\cos 2\Omega t + a_3\sin\Omega t+a_4\sin 2\Omega t , \tag{8}$$

where the coefficients a_i are combinations of invariant products of the vectors $\mathbf{e}$, $\mathbf{e}^*$ ϵ, ϵ^*, and $\mathbf{b}$. The coefficients a_i (for $i>0$) are responsible for effects periodic in time in the alignment term ("quantum beats").

For the sake of simplicity we restrict our considerations to the case of real polarization vectors, i.e., to linear

polarizations in both channels. Introducing the following notation for the vectorial invariants involved,

$$p=\mathbf{e}\cdot\boldsymbol{\epsilon},\quad p_d=(\mathbf{e}\cdot\mathbf{b})(\boldsymbol{\epsilon}\cdot\mathbf{b}),\quad p_m=(\mathbf{e}\times\boldsymbol{\epsilon})\cdot\mathbf{b}\ , \tag{9}$$

we arrive at the simple expressions:

$$a_0=(3p^2+9p_d^2+3p_m^2-6pp_d-2)/6\ , \tag{10a}$$

$$a_1=2(p-p_d)p_d\ , \tag{10b}$$

$$a_2=(p^2+p_d^2-p_m^2-2pp_d)/2\ , \tag{10c}$$

$$a_3=2p_dp_m\ , \tag{10d}$$

$$a_4=(p-p_d)p_m\ . \tag{10e}$$

They provide together with Eq. (6) a generalization of the well-known geometrical relations [8] in the case of arbitrary mutual orientation of the optical polarization vectors and magnetic field vector. It is easy to note that if any of the polarization vectors is parallel to the magnetic field, quantum beats vanish.

This general formalism of the TRLIF signal can now be used to discuss polarization and magnetic field effects in time-resolved fluorescence experiments and allows us to calculate theoretical decay curves with respect to the applied geometry of the present experiment and the atomic configuration of the levels under investigation.

III. EXPERIMENTAL SETUP

In Fig. 1 a sketch of the time-resolved laser-induced fluorescence experiment is shown, which is used in our laboratory for lifetime measurements [4,11,12,27]. The atomic or ionic beam, the exciting laser beam, and the observation axis are oriented at right angles. A low-pressure hollow cathode discharge similar to the one described by Duquette, Salih, and Lawler [30] is used as the atom and ion source. One end of the cathode is closed except for a 2-mm hole. The pressure of neon and argon in the discharge was typically several millibars, while the

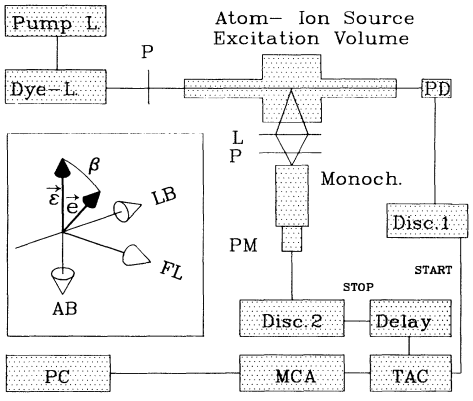

FIG. 1. Experimental setup and geometry of the TRLIF experiment. *P*, polarizer; *L*, imaging lens; PD, photodiode; PM, photomultiplier; TAC, time-to-amplitude converter; MCA, multichannel analyzer; PC, personal computer; LB, direction of laser beam; **e** and $\boldsymbol{\epsilon}$ are polarization vectors of laser and fluorescence light, respectively.

pressure in the excitation volume could be varied from 10^{-4} to 10 mbar by opening a needle valve in a bypass. Details of our atom and ion source are described elsewhere [27].

Two linear polarizers, one in the excitation and one in the observation channel, were used to get well-defined directions of polarization. The polarizer in the observation channel was fixed to transmit light with an electric vector directed vertically while that in the excitation channel could be rotated by an appropriate angle. A pair of coils enabled us to produce a homogeneous magnetic field up to 95 G in the direction of observation.

The levels under investigation were selectively excited by a dye laser system that was pumped by a N_2 laser or a XeCl-excimer laser. Special care was taken to ensure that the measured decay curves were not influenced by the duration of the exciting laser pulse. To that end we have developed dye lasers that produce single pulses with subnanosecond duration at repetition rates of up to 200 Hz [11,25,26]. They offer the possibility to measure lifetimes down to some hundreds of picoseconds without the need to deconvolute the exciting pulse from the fluorescence signal. For details the reader is referred to recent papers [11,12,26].

The fluorescence from the excitation volume was focused onto the slit of a monochromator. The photons were detected with a fast multiplier (Hamamatsu R928) followed by a standard photon-counting system. For measurements of lifetimes of a few nanoseconds a constant-fraction discriminator was used for the photomultiplier output, which gives the stop signal for the time-to-amplitude converter, to improve the resolution of the photon-counting system [11]. The mean counting rate was adjusted to about 0.1 photons per laser pulse to reduce the pileup effect. The width of the single channel in the multichannel analyzer was set to correspond approximately to one-tenth of the lifetime to be measured. With this setting the decay curves could be measured with good signal to noise ratio for roughly three to five lifetimes.

For reduction of the data stored in the computer the background was subtracted in a first step. Second, a correction was applied to account for a possible influence of the pileup effect. In the last step of the evaluation routine a straight line was fitted to the logarithm of the count rates instead of fitting an exponential curve to the data. This gives more weight to those channels with high counting rates.

IV. RESULTS AND DISCUSSION

A number of effects may influence the time evolution of the fluorescence signal in experiments using laser excitation and obstruct the determination of the natural lifetime. Collisions with other atoms in the observation chamber may disturb the accuracy of the measured lifetimes as well as radiation trapping, the escape of the excited atoms before detection of the fluorescence (flight-out-of-view effect), the finite width of the excitation pulse, the influence of the direction or polarization in the excitation and observation channel, and the influence of re-

sidual magnetic fields [4]. However, in most lifetime experiments which use the technique of time-resolved laser-induced fluorescence only one or two of these effects have been explicitly taken into account. Polarization effects and the influence of magnetic fields usually have been neglected completely.

A. Polarization effects

Selective excitation of atomic or ionic levels with unpolarized or linearly polarized light can produce alignment which is destroyed by collisions in the presence of disturbing atoms. The time evolution of the fluorescence signal then not only depends on the natural lifetime of the excited level but also on the number density of atoms in the observation chamber, on the cross section for alignment destroying collisions, and in the case of linearly polarized light also on the angle between the polarization in the excitation and the observation channel. In the following we only discuss the case of linearly polarized light, because then the alignment effects on time-resolved laser-induced fluorescence curves are expected to be more pronounced.

The time dependence of the alignment term [Eqs. (4) and (8)] which is caused by the collisional redistribution of population in the Zeeman manifold of the upper level can limit the accuracy of the lifetime data if it is not taken into account properly. The angular distribution function of the alignment term Eq. (8), which is highly sensitive to the geometry of the experiment [Eqs. (9) and (10a)–(10e)], is reduced in the absence of a magnetic field, and the TRLIF signal then takes the form [8]:

$$S(t)\sim \exp(-\Gamma t)\{\exp(-\Gamma_0^{\mathrm{coll}}t) + \alpha(2)\exp(-\Gamma_2^{\mathrm{coll}}t)(3\cos^2\beta-1)\}\ , \tag{11}$$

where the angle β is formed by the polarization vectors $\mathbf{e}$ and $\boldsymbol{\epsilon}$ of the laser beam and the fluorescence light, respectively (refer to Fig. 1). It is well known that for the so-called "magic angle" $\beta=54.7°$ the second (alignment) term in (11) vanishes.

To demonstrate the importance of the alignment term on the time evolution of the fluorescence signal we discuss in the following the influence of different $\alpha(2)$ coefficients and different ratios of the collisional relaxation constants for depopulation and disalignment. In order to do that we calculate and plot the ratio S_2/S_1 of the fluorescence intensities for excitation under an arbitrary angle (β_2) to that under "magic angle" (β_1). From Eq. (11) we get

$$S_2/S_1=1+\alpha(2)(3\cos^2\beta_2-1)\exp\{-(\Gamma_2^{\mathrm{coll}}-\Gamma_0^{\mathrm{coll}})t\}\ . \tag{12}$$

For a quantitative estimate we have deduced cross sections for depopulation and disalignment from our experimental results for the neon I $3p'[1/2]_1$ level. We obtain $\sigma_0^{\mathrm{coll}}=5.6\times10^{-17}$ cm^2 and $\sigma_2^{\mathrm{coll}}=3.7\times10^{-15}$ cm^2. Thus, we have for the ratio $P=\Gamma_0^{\mathrm{coll}}/\Gamma_2^{\mathrm{coll}}=0.015\ll1$. Assuming that this approximation holds for the specific transition one is interested in we can write

$$(\Gamma_2^{\mathrm{coll}}-\Gamma_0^{\mathrm{coll}})=\Gamma_2^{\mathrm{coll}}(1-P)\approx\Gamma_2^{\mathrm{coll}}\ . \tag{13}$$

For a general presentation of the results it is convenient to express the time in units of the natural lifetime of the respective level and to express the collisional relaxation rate in terms of the inverse lifetime. Thus with $q=t/\tau$ and $r=\Gamma_2^{\mathrm{coll}}/\Gamma$ we obtain:

$$(\Gamma_2^{\mathrm{coll}}-\Gamma_0^{\mathrm{coll}})t\approx rq\ . \tag{14}$$

We can now rewrite Eq. (12):

$$S_2/S_1=1+\alpha(2)(3\cos^2\beta_2-1)\exp(-rq)\ . \tag{15}$$

In Figs. 2(a) and 2(b) we present the results for the ratios of the intensities according to Eq. (15) for two extreme angles $\beta_2=0°$ and 85°. The angle of 85° instead of 90° was chosen because if the polarization vectors of the exciting laser and of the fluorescence light are crossed then, for $\alpha(2)=1$, no signal in the case of negligible collisions is observed. No or only a poor signal is obtained in the case of collisions, especially when the fluorescence just starts.

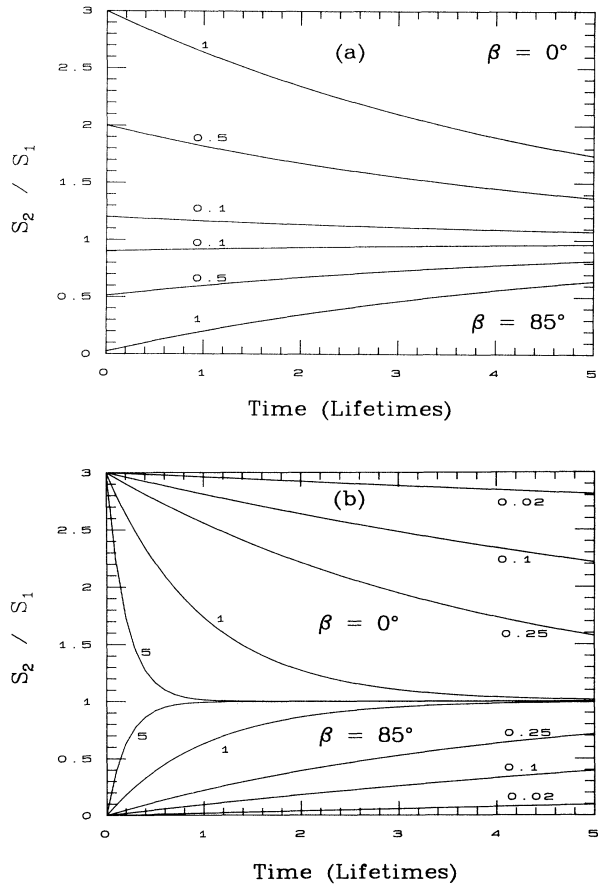

FIG. 2. (a) Time evolution of the ratio of the fluorescence intensities according to Eq. (15) for two extreme angles $\beta_2=0°$ and 85°. This ratio is shown for different $\alpha(2)$ coefficients but constant ratio of $r=\Gamma_2^{\mathrm{coll}}/\Gamma$. (b) Time evolution of the ratio of the fluorescence intensities according to Eq. (15) for two extreme angles $\beta_2=0°$ and 85°. This ratio is shown for constant anisotropy parameter $\alpha(2)=1$ and different ratios of $r=\Gamma_2^{\mathrm{coll}}/\Gamma$.

The smaller the value of $\alpha(2)$ is the larger is the initial value of the fluorescence signal in that case.

The time evolution is shown for five lifetimes which is a usual observation time in lifetime experiments using laser-induced fluorescence. To analyze properly Figs. 2(a) and 2(b) one should remember that the lifetime is calculated from the slope of the TRLIF signal. Thus, a deviation of the measured lifetime from the natural one is expected when the slope of the curves calculated for the ratios S_2/S_1 differs from zero, while a deviation of this ratio from the value $S_2/S_1=1$ represents a difference in the intensities between the signals S_2 and S_1 only.

In Fig. 2(a) the coefficient $\alpha(2)$ was varied for a fixed value of $r=\Gamma_2^{\text{coll}}/\Gamma=0.2$. The largest deviation from the "magic-angle" excitation signal is observed for the transition scheme $J=0\rightarrow J=1\rightarrow J=0$ ($\lambda_L=\lambda_D=616.36$ nm), in which the excitation starts from the same state on which the observed fluorescence ends. In this case the anisotropy coefficient $\alpha(2)$ reaches its maximum value of 1. Even if only the second half of the decay curve is taken for calculating the lifetimes the slope of the S_2/S_1 curve differs considerably from the value zero and a systematic error will appear in the derived lifetimes. Quite different is the situation for the same upper level when another transition scheme is used. For $J=0\rightarrow J=1\rightarrow J=2$ ($\lambda_L=616.36$ nm, $\lambda_D=588.19$ nm) the coefficient $\alpha(2)=0.1$ and the deviation from the "magic-angle" excitation signal is negligible even at the starting point of the decay curve. In Fig. 2(a) curves for polarization angles $\beta_2=0°$ and 85° are shown. The general influence on the decay curves is quite the same in both cases, except that the curvature has the opposite sign and that in the logarithmic presentation the deviation from a straight line is less pronounced for $\beta_2=0°$. Therefore we have chosen for the experiments $\beta_2=85°$.

In Fig. 2(b) also curves for the ratio S_2/S_1 are shown. Here the transition scheme $J=0\rightarrow J=1\rightarrow J=0$ is fixed and the ratio $r=\Gamma_2^{\text{coll}}/\Gamma$ is changed. Now, we can observe that for two extreme values of r the results are similar: If r is large ($r=5$ in the figure) the slope tends to 0 very fast and, except for the starting part, it is close to the signal observed with "magic-angle" excitation. Also when r is very small ($r=0.02$ in the figure) the slope is very small but in this case it is almost constant in time. In both cases the evaluation of the curve will give a lifetime close to that taken with "magic-angle" excitation despite significant differences of the signal intensities for cases of small values of r.

For the intermediate values of r even the evaluation of the second half of the decay curve observed by excitation without a "magic angle" will give a lifetime that differs significantly from the proper value.

These illustrations show that the influence of the alignment term on the time-resolved fluorescence signal depends very sensitively on the transition scheme involved and also on the value of the cross section for alignment destroying collisions. Often no direct influence can be observed on the measured decay curves but still the accuracy of the lifetime data is limited by the laser-induced alignment. This may be an explanation why effects resulting from excitation anisotropy with linearly polarized laser light have been neglected in most lifetime experiments so far.

In the following we will discuss some experimental results that will directly show an influence of the alignment term on the time evolution of the fluorescence signal. For this investigation we have chosen the neon I transition $3s'[1/2]_0$-$3p'[1/2]_1$ for excitation and also for observation of the fluorescence signal ($\lambda_L=\lambda_D=616.36$ nm). Then $\alpha(2)=1$ and we expect the largest effect. We present the results only for $\beta_2=85°$ because in that case specific features of the alignment dependent effects are more pronounced.

We have to distinguish between two cases: the collision free case and the one when collisions with other atoms in the excitation chamber become important. The first one is realized for pressures in the excitation volume below 10^{-4} mbar. Collisions of excited neon atoms with other atoms are then less important because of the low number density and the rather small depopulation cross section of the neon I $3p'[1/2]_1$ state ($\sigma_0^{\text{coll}}=5.6\times10^{-17}$ cm^2). The rate Γ_k^{coll} is then small compared to Γ, thus Γ_k approaches Γ with good accuracy. The exponential decay of the observed fluorescence signal is then independent of the alignment and therefore it is described only by the natural lifetime $\tau=1/\Gamma$ In Fig. 3(a) this case is shown for the measured fluorescence signal of this neon I level.

The evaluation of the decay curves by linear regression with a computer routine gives for $\beta=54.7°$ a lifetime of $\tau=18.5$ ns and for $\beta=85°$ a lifetime of $\tau=18.7$ ns. Both values are in good agreement within the experimental uncertainties.

This confirms that the polarization of the exciting laser light does not influence the time evolution of the fluorescence signal when collisions are negligible, but it does modify the intensity of the signal. In the case of almost crossed polarizers ($\beta=85°$) the signal is about 10 times weaker than that observed for $\beta=54.7°$ under the same conditions. For the same considerations synthetic decay curves have been calculated that are shown in Fig. 3(b). They agree with the experimental ones in so far as both have the same slope but significantly different intensities. It is difficult to compare the absolute values because the simulations only make use of the number densities and the atomic constants whereas in the experimental data losses in the apparatus will influence the intensity of the fluorescence light and make a quantitative comparison difficult.

The same calculations and measurements have been performed for this neon I transition when collisions with other neon atoms become important. This is realized for pressures in the excitation volume above 1 mbar. In this case the exponential decay of the fluorescence is described by the rates $\Gamma, \Gamma_0^{\text{coll}}$, and Γ_2^{coll} [Eq. (11)]. Thus, the depopulation as well as the alignment term cannot be neglected any longer.

In Fig. 3(c) the measured decay curves for this level are shown. The polarization angle β is again given as parameter. In the semilogarithmic plot a straight line is observed for excitation with $\beta=54.7°$ while for $\beta=85°$ a

nonlinear dependence is obtained. The evaluation of the curve taken by "magic-angle" excitation gives a lifetime of $\tau = 18.3$ ns when fitting the data points to a single exponential. This is in very good agreement with the low-pressure result. For these experimental conditions we have also calculated synthetic decay curves that are shown in Fig. 3(d). Again the qualitative behavior of the experimental data is nicely reproduced.

As further illustration a decay curve of the $3p'[1/2]_1$ level is shown in Fig. 3(e) when the transition scheme $J=0 \rightarrow J=1 \rightarrow J=2$ is used for excitation and observation. This results in $\alpha(2)=0.1$. The polarization angle was $\beta=85°$ and the pressure in the excitation volume was $p=1$ mbar. In the semilogarithmic plot a straight line is

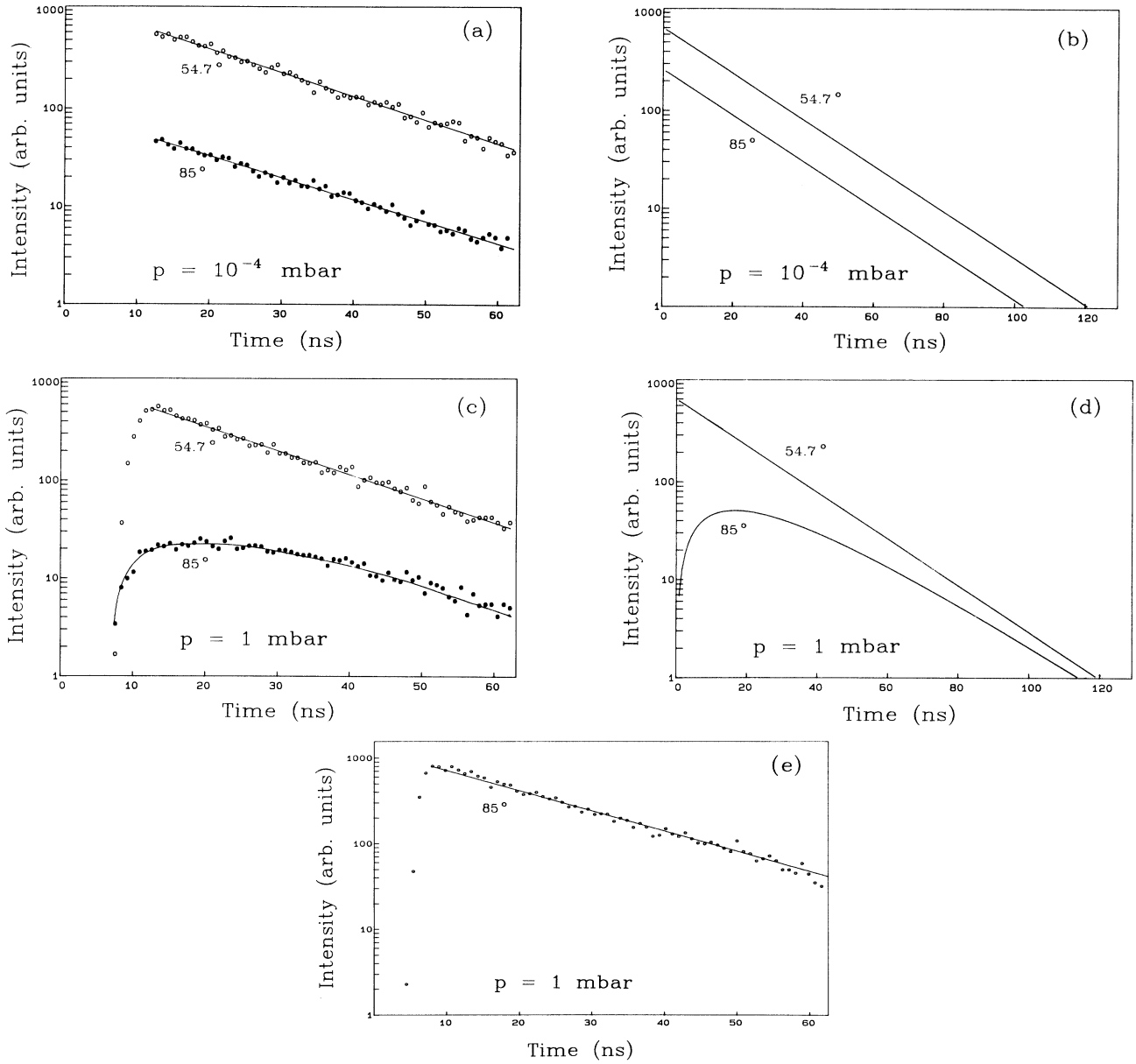

FIG. 3. (a) Temporal shape of the neon I $3p'[1/2]_1$ fluorescence signal observed for $p=10^{-4}$ mbar and two different values of the angle β, as indicated. For excitation and observation the transition scheme $J=0 \rightarrow J=1 \rightarrow J=0$ ($\lambda_L = \lambda_D = 616.36$ nm) is used. For $\beta=54.7°$ a lifetime of 18.5 ns and for $\beta=85°$ a lifetime of 18.7 ns is observed, which is in good agreement within the experimental uncertainties. (b) Theoretical decay curves calculated for the low-pressure condition for the same transition and the same values of β as in (a). (c) Temporal shape of the fluorescence signal observed for $p=1$ mbar, transition scheme and angles as before. For $\beta=54.7°$ a lifetime of 18.3 ns is derived. (d) Theoretical decay curves for the high-pressure condition for the same transition and the same values of β as in (c). (e) Temporal shape of the fluorescence signal observed for $p=1$ mbar and $\beta=85°$ when the transition scheme $J=0 \rightarrow J=1 \rightarrow J=2$ is used for excitation and observation ($\lambda_L = 616.36$ nm, $\lambda_D = 588.19$ nm). The fitted line represents a lifetime of 18.2 ns.

then observed for the decay signal. Fitting the data points by linear regression we get a lifetime of $\tau=18.2$ ns which is in good agreement with the result taken at 1 mbar and the transition scheme $J=0\rightarrow J=1\rightarrow J=0$ and $\beta=54.7°$. This confirms also the theoretical prediction shown in Fig. 2(a).

The quenching effect does not disturb a single exponential decay in these cases because Γ_0^{coll} adds simply to Γ. Due to the low depopulation cross section for this level the influence is small. To show the influence of collisions experiments at even higher pressure have been carried out and the collision free lifetime for this state has been determined from a Stern-Vollmer plot. The results of these measurements where the pressure was varied from 10^{-4} to 10 mbar are shown in Fig. 4(a). From the slope of the fitted line a cross section for depopulation of $\sigma_0^{\text{coll}}=5.6(6)\times10^{-17}$ cm^2 is derived for $T=300$ K, which is in good agreement with the value given by Fujimoto, Goto, and Fukuda [14].

It is also interesting to note that the excitation of the $3p'[1/2]_1$ level with linearly polarized laser light at $\beta=85°$ makes it possible to measure the disalignment rate Γ_2^{coll} from the time-resolved fluorescence signal with the same experimental setup. The data points then have to be fitted to Eq. (11). A result of this procedure is shown in Fig. 4(b). We obtain for the collisional disalignment rate of this neon I level $\Gamma_2^{\text{coll}}=1/95.1$ ns^{-1} for $p=1.5$ mbar.

The shape of the curve for excitation with $\beta=85°, p=1$ mbar, and $\alpha(2)=1$ [Figs. 3(c) and 3(d)] can be explained by a population transfer from the Zeeman sublevel $m_J=0$ to those with $m_J=\pm1$ in the excited $3p'[1/2]_1$ state caused by collisions. For the chosen transition scheme ($J=0\rightarrow J=1\rightarrow J=0$) there is a straightforward classical interpretation. The excitation with linearly polarized laser light populates the sublevel with $m_J=0$. The only allowed transition from that level has an electric dipole moment parallel to the pumping electric vector and thus is almost perpendicular to the direction of observation ($\beta=85°$). That means this transition cannot be observed directly. Isotropic collisions destroying an alignment cause the population transfer to sublevels with $m_J=\pm1$ (Fig. 5). Due to this process we can detect the fluorescence signal which originates from these collisionally populated sublevels. The observed increase of the fluorescence intensity at the beginning indicates that the disalignment process (population transfer among the Zeeman sublevels) is slower than the radiative depopulation of the excited level.

The evaluation of the fluorescence curves which have been measured in this case will give systematically too long lifetimes even if data are taken only from the second half of the decay curve [refer to Fig. 3(c)].

In conclusion, we summarize as follows. In the presence of collisions only "magic-angle" excitation gives the undisturbed time evolution of the fluorescence signal. Measurements performed with other angles β will give different lifetimes. The magnitude of the influence of laser-induced alignment depends very sensitively on the chosen transition scheme, on the value of the cross sec-

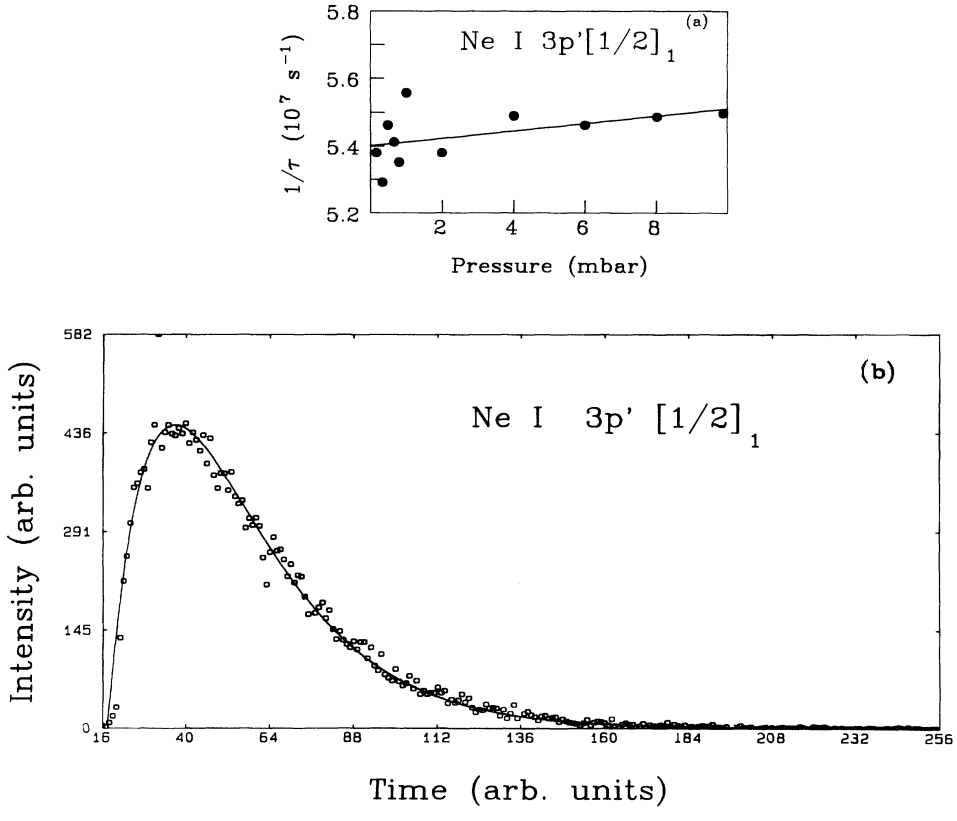

FIG. 4. (a) Stern-Vollmer plot of the neon I $3p'[1/2]_1$ level. The zero-pressure extrapolation gives $1/\Gamma=\tau=18.5$ ns. (b) Temporal shape of the neon I $3p'[1/2]_1$ fluorescence signal measured for $\beta=85°$ and a pressure of $p=1.5$ mbar in the excitation volume. The dots representing the measured data and the line is a chi-square fit which gives for the collisional disalignment rate $\Gamma_2^{\text{coll}}=1/95.1$ ns^{-1}.

tion for alignment destroying collisions and on the geometry of the experiment. The capability of the TRLIF method to measure in combination with short laser-pulse excitation disalignment rates is also demonstrated for the neon I $3p'[1/2]_1$ level.

In the collision free case a proper choice of the polarization in the excitation and observation channel can be used to optimize weak fluorescence signals, because the angle between the polarization directions in this case only changes the intensity and not the time evolution.

B. Magnetic fields

The fluorescence signal of an ensemble of aligned atoms will contain an oscillatory term in addition to the exponential terms due to the decay of population and alignment if a magnetic field is present. In the case under consideration the magnetic field points into the direction of observation and all three vectors **b**, **e**, and ϵ are in the same plane; thus the parameters p_d and p_m as well as the function $F_1(t)$ vanish [refer to Eqs. (6) and (9)]. Equation (4) then takes the form

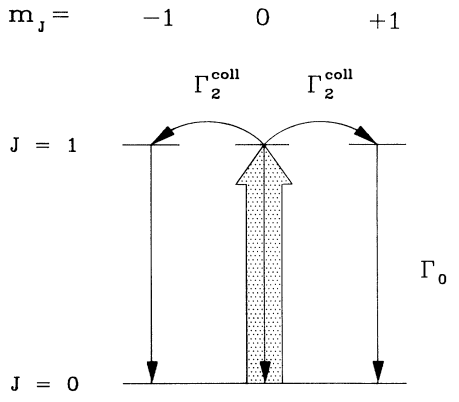

FIG. 5. The linearly polarized laser pulse (arrow pointing upwards) creates population (alignment) of the $m_J=0$ Zeeman sublevel of the $J=1$ state when starting the optical pumping from a $J=0$ state. Collisions redistribute the population with a rate Γ_2^{coll} among all sublevels and stimulate depopulation with a rate Γ_0^{coll}.

$$S(t)\sim \exp(-\Gamma t)\{\exp(-\Gamma_0^{\text{coll}}t)+\tfrac{1}{2}\alpha(2)\exp(-\Gamma_2^{\text{coll}}t)[(3\cos^2\beta-2)+3\cos^2\beta\cos 2\Omega t]\}\ , \tag{16}$$

where $\Omega=2\pi g_J\mu_B B/h$ is the Larmor frequency.

Problems may arise even with very weak fields such as, for instance, the Earth's magnetic field or stray fields from the laboratory equipment. They may cause the Larmor period to become comparable to the lifetime value. Then the measured decay constant of the fluorescence signal will differ from the natural lifetime. On the other hand, if the period of these oscillations is short compared to the lifetime an average over these oscillations is performed in the evaluation routine and the correct lifetime should be observed. But also here problems may arise that will be discussed later.

The influence of the Earth's magnetic field is demonstrated for the argon I $5p[5/2]_2$ level with a lifetime of $\tau=154(7)$ ns [4]. The polarizer in the observation channel was orientated with its transmission in vertical direction and the one in the excitation channel was at "magic-angle" position. The pressure in the excitation volume was 10^{-4} mbar. The influence of laser-induced alignment on the time-resolved fluorescence signal is then negligible [refer to Fig. 3(a)]. In Fig. 6 an experimental decay curve of the argon I $5p[5/2]_2$ level is shown. The excitation was performed at $\lambda_L=419.07$ nm and the fluorescence was observed at $\lambda_D=430.01$ nm. The time of observation of the decay signal corresponds to approximately four lifetimes. In the semilogarithmic plot a deviation from a straight line which is expected in the case of a simple exponential decay is observed. This is due to the influence of the Earth's magnetic field. Now the measured fluorescence signal is described by Eq. (16). For our experimental conditions the rate Γ_2 can here be approximated by the rate Γ. When fitting the data points shown in Fig. 6 to Eq. (16) we observe for the decay time $1/\Gamma_0=151$ ns and for the Larmor frequency $\Omega=5.9$ MHz. This corresponds to the component of the Earth's magnetic field pointing into the direction of observation in our experiment. The line in Fig. 6 is the result of this fit.

The influence of magnetic fields on the time evolution of the fluorescence signal has also been investigated for the case when laser-induced alignment is not negligible anymore. As an example we have chosen again the neon I $3p'[1/2]_1$ state. The orientation of the polarizer in the observation channel was the same as described before

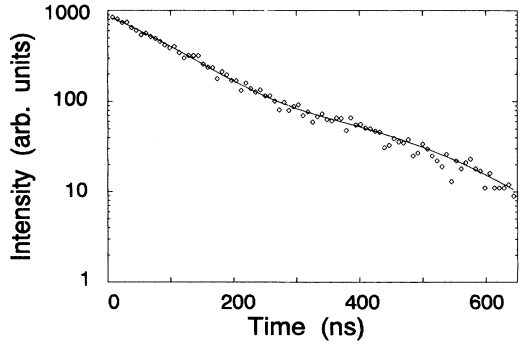

FIG. 6. The influence of the Earth's magnetic field on the time-resolved laser-induced fluorescence signal of the argon I $5p[5/2]_2$ level. The excitation was performed at $\lambda_L=419.07$ nm and the observation of the fluorescence at $\lambda_D=430.01$ nm. The pressure in the observation chamber was $p=10^{-4}$ mbar. The line represents a fit of the data points to Eq. (16). A lifetime of $\tau=151$ ns and a Larmor frequency of $\Omega=5.9$ MHz is observed.

whereas the one in the excitation channel was set to $\beta=0°$, $\beta=54.7°$, or $\beta=90°$ [upper, middle, or lower curves in Figs. 7(a) and 7(b)] with respect to the vertical axis. For excitation and observation we have used the transition scheme $J=0\rightarrow J=1\rightarrow J=0$ ($\lambda_L=\lambda_D=616.36$ nm), resulting in $\alpha(2)=1$. The pressure in the excitation volume was $p=4$ mbar for these measurements. In direction of observation a magnetic field with $B=15$ G was applied. The experimental data are shown in Fig. 7(a). For the polarization angles $\beta=0°$ and $\beta=54.7°$ a modulation of the fluorescence signal with the Larmor frequency $\Omega=1.8\times10^8\ s^{-1}$ is observed while for $\beta=90°$ the oscillatory term in Eq. (16) vanishes and the decay signal is free of oscillations. Then the time evolution of the fluorescence signal can be described by the rates Γ, Γ_0^{coll}, and Γ_2^{coll}. When fitting this decay curve to Eq. (16) we observe for the rate of alignment destroying collisions $\Gamma_2^{coll}=3\times10^7\ s^{-1}$. The experimental data in Fig. 7(a) also show a decrease of the intensity of the maxima of the oscillations in the fluorescence signal when changing the angle of polarization from $\beta=0°$ to $\beta=90°$ in the experiment while the intensities of the minima of the oscillations are not influenced by the value of the polarization angle β. Therefore, if a magnetic field is present in the direction of observation the minima of the resulting oscillations of the fluorescence signal can always be fitted to Eq. (11). This is independent of the angle of polarization β.

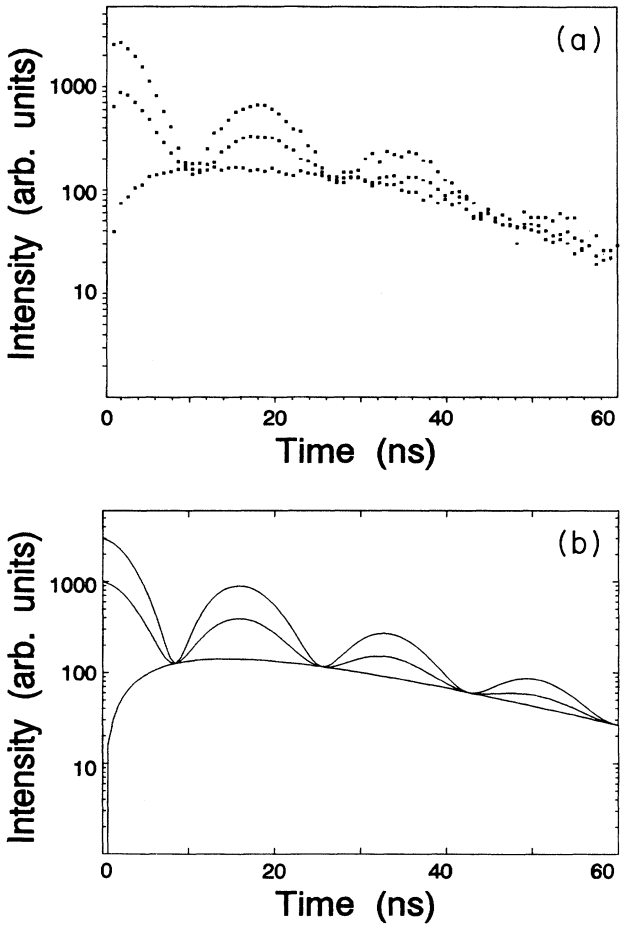

FIG. 7. The influence of external magnetic fields on the time-resolved fluorescence signal of the neon I $3p'[1/2]_1$ state. The excitation and observation was performed at $\lambda_L=\lambda_D=616.36$ nm. The pressure in the excitation volume was $p=4$ mbar and the magnetic field strength was 15 G pointing into the direction of observation. The decay signals were measured (a) for the polarization angles $\beta=0°$, 54.7°, and 90° (upper, middle, and lower curves) and also simulated (b) for the experimental conditions by calculating Eq. (16).

In Fig. 7(b) a simulation of Eq. (16) is shown for the experimental conditions as described above. A very nice agreement with the experimental data is observed both in the time evolution and in the overall magnitude of the fluorescence signals.

Afterwards lifetime measurements have been performed for different external magnetic field strengths and fixed pressure in the excitation volume. The ratio of measured lifetimes with (τ_B) and without any magnetic field ($\tau_B=0$) is shown in Fig. 8 for the argon I $5p[5/2]_2$ (solid dots) and the neon I $3p'[1/2]_1$ (open dots) states. The gas pressure in the excitation volume was fixed at 2×10^{-4} mbar for these measurements and the hollow cathode discharge was operated with a current of $I=1$ A. For both states a systematic shortening of the measured lifetime with increasing magnetic field strength is observed. When increasing the magnetic field up to 95 G a shortening of 9% was observed for the argon level, while for neon and same experimental conditions the shortening was only 6%.

This observation is interesting in so far as the application of strong magnetic fields is a common method to suppress influences of weak magnetic fields or the alignment term on the decay curves when Zeeman beats are present and $\beta=54.7°$. Numerous examples can be found in the literature describing this type of time-resolved fluorescence experiments [8,14,15,31–33]. A number of alternative geometries for the vector of the magnetic field and the one for the polarization can be used to eliminate the influence of the beats on the fluorescence decay [8]. When using one of these geometries in the lifetime experiment the total alignment term becomes oscillatory. If the external magnetic field is strong enough the Larmor period can become much shorter than the lifetime. Then the oscillations will be smeared out if the time constant of the detection system is not sufficient for resolving the beats. The observed decay curve is then believed to be that of the population only [8].

However, the results presented in Figs. 7 and 8 show that this is not necessarily true. The application of an external magnetic field leads to a gyration of the charged particles in the atom and ion beam that leaves the hollow cathode discharge and expands into the observation chamber. In a first approximation it is believed that this beam is effusive [32,34]. Therefore it is assumed that in the case of $B=0$ G the atoms and ions in the beam have nearly the same velocity. When applying a magnetic field perpendicular to that beam and in the direction of observation the charged particles are gyrating around the field lines. Then the probability for collisions of the excited

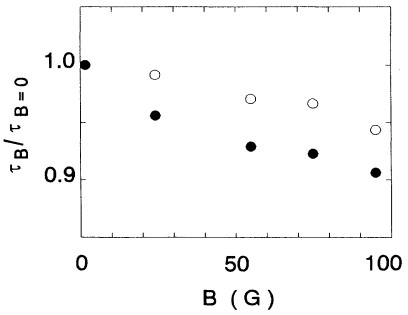

FIG. 8. Ratio of measured lifetimes with (τ_B) and without any external magnetic field ($\tau_{B=0}$) for the argon I $5p[5/2]_2$ (solid dots) and the neon I $3p'[1/2]_1$ (open dots) states. The pressure in the excitation volume was 2×10^{-4} mbar.

atoms with charged particles in the beam will be increased. This process will become more effective when the time for one gyration period of the charged particles is shorter than the lifetime of the observed excited atomic level. This may also be an explanation why the shortening of the argon level with a lifetime of $\tau=154$ ns is more pronounced compared to the neon lifetime with $\tau=18.5$ ns when the magnetic field strength is increased. This effect was also investigated in our laboratory when measuring the lifetime of the Cr II $z\,^6P^o_{7/2}$ state [12]. The lifetime of this level is $\tau=2.5(1)$ ns. No systematic change of the measured lifetimes was observed when increasing the magnetic field strength up to $B=25$ G (refer to Fig. 2 in Ref. [12]).

On the other hand, the number density of charged particles in the beam that is expanded from the hollow cathode into the vacuum chamber was changed. This is done in our experiment by reducing the current of the hollow cathode discharge. For the lowest current of $I=15$ mA the shortening of the argon lifetime of the $5p[5/2]_2$ level is observed to be 3% only for a field strength of $B=95$ G [35].

In a recently published paper we have reexamined the lifetime of the argon I $5p[5/2]_2$ level [4]. The value measured in our experiment was about 17% longer than the one measured in the experiment of Hirabayashi *et al.* [31]. In their experiment they have also used time-resolved laser-induced fluorescence for lifetime determination. The gas pressure in the plasma discharge used in their experiment was 0.12–2.7 mbar, while we have performed the lifetime measurements at very low pressures ($p=2\times10^{-4}$ mbar) [4]. Then alignment effects on the decay curves are negligible in our case, as is shown in the present investigation. Hirabayashi *et al.* [31] have eliminated alignment effects on their decay curves by applying a magnetic field of about 40 G into the direction of observation.

In general a shortening of the lifetime is caused by quenching effects. Collisional depopulation in a lifetime experiment as the present is eliminated by extrapolation to zero pressure in a Stern-Vollmer plot [refer to Fig. 4(a)]. This procedure only takes collisions of the excited states into account which occur with the rest gas (here the rare gas). However, as demonstrated in this investigation, the excited neon and argon states could be subjected to increased collisions with the charged particles in the beam when applying a magnetic field in the direction of observation. This collisional depopulation is not considered in a zero-pressure extrapolation of a Stern-Vollmer plot and therefore it may lead to systematically too short lifetime values. When performing lifetime measurements in a plasma discharge similar to that of Hirabayashi *et al.* [31] or that of Hannaford and Lowe [8] not only collisions of the excited state with ions but also with electrons may be important. For instance, the application of a magnetic field of about 20 G has been used in a recent experiment in our laboratory to increase the number density of some low lying metastable states of the chromium ion[12]. We believe that the gyrating electrons in the inside of the hollow cathode are responsible for this excitation mechanism. Therefore in the presence of a magnetic field of several Gauss the excited state may also be subject to collisions with electrons when performing lifetime measurements in a plasma discharge. These collisions may be responsible for the shortening of the argon lifetime in the experiment of Hirabayashi *et al* [31], and they are not considered in a Stern-Vollmer plot as shown in this investigation.

As a conclusion of this part we summarize as follows. Contrary to the laser-induced alignment of the upper-level population no "magic angle" exists to cancel influences due to external magnetic fields. The only method to avoid any influence is to compensate existing magnetic fields. In all other cases one has to evaluate the decay curves by fitting the data points to Eq. (16). The superposition of a low magnetic field by a stronger one may lead to wrong lifetime results as demonstrated in Fig. 8.

ACKNOWLEDGMENTS

This work was supported by the Deutsche Forschungsgemeinschaft (DFG). We wish to thank Professor D. Schlüter for helpful discussions and M. Raeth for his assistance during some of the measurements. One of us (L.W.) wishes to thank the University of Kiel for hospitality during a part of these studies and the Polish Government for support under Research Project No. CPBP 01.12.5.6.

APPENDIX A

In this appendix we give a theoretical analysis of the TRLIF signal using the graphical technique of the angular momentum theory [16–22]. In Figs. 9 and 10 we summarize the most important definitions and relations of the angular momentum diagrams and some basic operations. They follow mainly those used by Varshalovich, Moskalev, and Khersonskii [18] and the reader is referred to this source for details.

Equation (3a) is the starting point for our graphical

analysis of the TRLIF signal in terms of JVL diagrams. Performing elementary operations [Figs. 10(d) and 10(e)] on this graph we get it expressed by scalar products of the irreducible components of the density and detection operators,

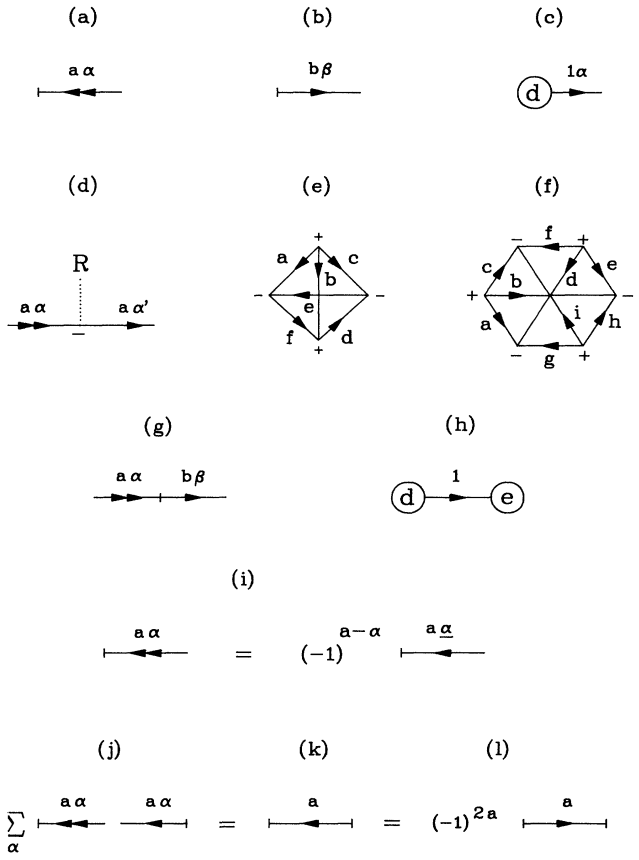

FIG. 9. Basic definitions of the angular momentum diagrams. (a) $\langle a\alpha|$, "bra" state vector; (b) $|b\beta\rangle$, "ket" state vector. (c) The α component of a vectorial operator $\mathbf{d}$. (d) The Wigner matrix element $D^{a}_{\alpha\alpha'}(R)$ of the rotation R. (e) The Wigner $6j$ symbol

$$\begin{Bmatrix} abc \\ def \end{Bmatrix}.$$

(f) The Wigner $9j$ symbol

$$\begin{Bmatrix} abc \\ def \\ ghi \end{Bmatrix}.$$

(g) The scalar product $\langle a\alpha|b\beta\rangle$ of two state vectors. (h) The invariant (scalar) product $\mathbf{d}\cdot\mathbf{e}$ of two vectorial operators—prototype for the invariant product of any tensorial operators. Omitted internal labels are summed. (i) Transformation from "bra" into "ket" vector ($\boldsymbol{\alpha}=-\alpha$). (j)–(k) The projection operator onto the manifold $\{a\}$. (l) Reversion operation of the arrow.

$$S(t) = \sum_{k} \left(\rho_s \xrightarrow{k} D\right), \tag{A1}$$

where $\rho_s=\rho_s(t)$ is the density matrix of the manifold $\{s\}$. The contragredient spherical components of the 2^k multipole moment of this density matrix are [23,24]

$$\overset{k}{\rho}_{s\kappa}(t) = \left(\rho \xrightarrow{s} \hat{k}\kappa \xrightarrow{s'}\right) = \left(\rho_s \xrightarrow{k\kappa}\right). \tag{A2}$$

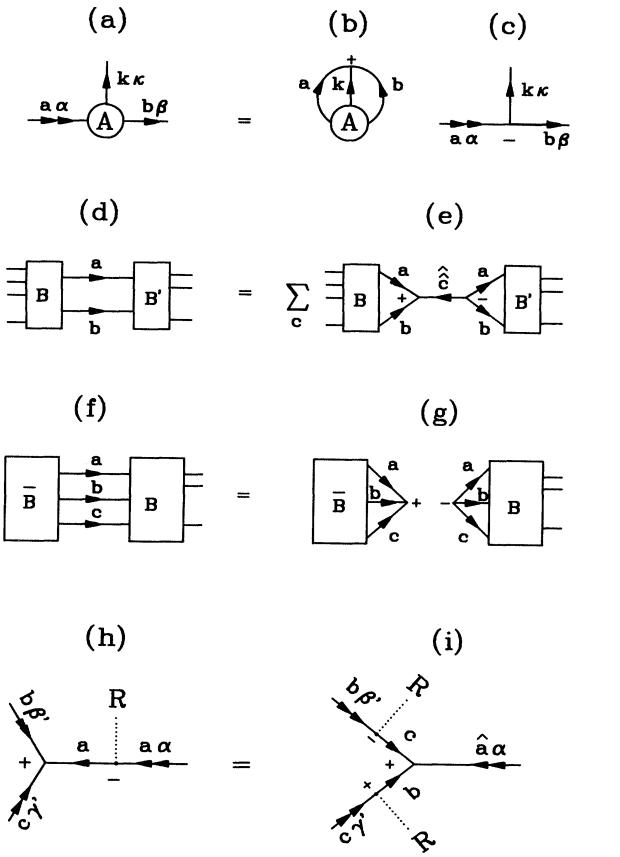

FIG. 10. Elementary operations on JLV diagrams. (a)–(c) Wigner-Eckart theorem. (a) The matrix element of the rank k spherical operator A between states $\langle a\alpha|$ and $|b\beta\rangle$. (b) The reduced matrix element $(a\|A^{k}\|b)$ of the operator A. (c) The Wigner $3j$ symbol with a phase factor

$$(-1)^{a-\alpha}\begin{Bmatrix} akb \\ \alpha\kappa\beta \end{Bmatrix}.$$

(d)–(e) Decomposition of two and (f)–(g) of three (the graphical JLV-3 theorem [18,21]) lines connecting two blocks of diagrams. The block $\bar{B}$ has all other lines closed; $\hat{c}=(2c+1)^{1/2}$ and $\hat{\hat{c}}=2c+1$. (h)–(i) The Clebsch-Gordan expansion of the Wigner D function [18]:

$$\sum_{\alpha'}\begin{Bmatrix} a\ b\ c \\ \alpha'\beta'\gamma' \end{Bmatrix} D^{a*}_{\alpha'\alpha}(R) = \sum \begin{Bmatrix} abc \\ \alpha\beta\gamma \end{Bmatrix} D^{b}_{\beta'\beta}(R) D^{c}_{\gamma'\gamma}(R).$$

These states multipoles transform according to the irreducible representations D^{k*} of the rotation group and have well-known interpretations [7,24] for values of k up to 2. The scalar ($k=0$) part ρ_s is related to the population of the excited state $\{s\}$. The vectorial ($k=1$) part ρ_s originates in the asymmetry in population of the Zeeman sublevels of $\{s\}$ with different signs of their magnetic quantum numbers (orientation) and is proportional to the mean magnetic moment in this manifold. The tensorial ($k=2$) part ρ_s stands for the difference in population of sublevels having different absolute values of their magnetic numbers (alignment) and is proportional to the mean electric quadrupole moment in the state considered.

1. Reduction of the detection operator

The irreducible components of the detection operator

$D^{(\epsilon)}_{k\kappa} =$ 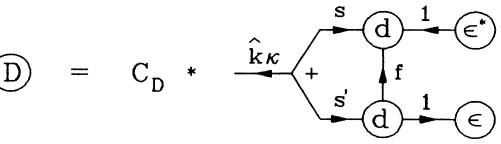 (A3)

take with regard to the Wigner-Eckart theorem [Figs. 10(a)–10(c)] and on recoupling of the angular momenta [Figs. 10(d)–10(g)] the form

$D^{(\epsilon)}_{k\kappa} =$ 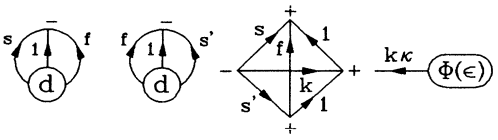 (A4)

where the geometrical part of the detection operator is given as an irreducible product of the complex polarization vectors in the detection channel:

$\Phi_{k\kappa}(\epsilon) =$ 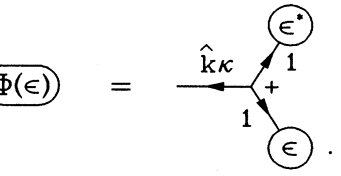 (A5)

This may be treated as the irreducible component of the coherency matrix of the fluorescence light. Since the polarization vectors are of rank 1, the values of the label k range from 0 up to 2 due to the "triangular condition." Thus, only the signal from the three state multipoles of these ranks can be detected in the fluorescence experiment.

2. Absorption operator

We consider an atomic system under the action of a laser pulse in the presence of a constant magnetic field **B**. We ignore hyperfine-structure coupling but generalization covering this case based on the results of Luypaert and VanCraen [22] is straightforward.

We assume that the mean value of the laser light wavelength λ_L corresponds to transitions between unperturbed multiplets $\{g\}$ and $\{s\}$, whereas the bandwidth of the pulse is broad enough to cover the whole spectral range of these transitions broadened by the simultaneous interaction of the atom with the magnetic field, the radiation field and other atoms (broadband excitation). Under these conditions the process of optical pumping from the states $\{g\}$ into $\{s\}$ can be described using the absorption operator [24] $A(\tau)$, which is in graphical notation,

$A(\tau) =$ 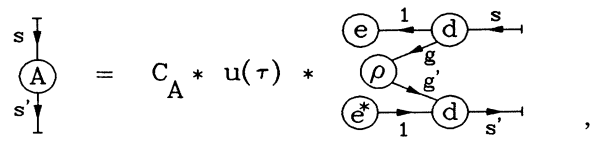 (A6)

where **e** is the polarization vector of the pumping light propagating into the direction k_L. The instantaneous energy density $u(\tau)$ of the laser pulse at the moment τ is assumed to be constant within the spectral region of optical transitions between these two manifolds. The constant C_A will be omitted as previously the constant C_D. Owing to the Wigner-Eckart and the recoupling theorems [Figs. 10(a)–10(e)] the irreducible form of the absorption operator can be written as

$$A^k_\kappa(\tau) = \text{(A)}\overset{k\kappa}{\longleftarrow} = u(\tau) * \text{(d)}\,\text{(d)} \sum_j \text{(e)}\,\text{(e*)}\,\text{(}\rho_g\text{)} \qquad \text{(A7)}$$

and finally due to the JLV-3 theorems [Figs. 10(f) and 10(g)] as

$$A^k_\kappa(\tau) = p(\tau) * \sum_{j,l} \qquad \text{(A8)}$$

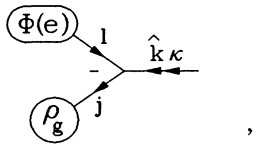

where the function $p(\tau)$ describing the efficiency of optical pumping contains the function $u(\tau)$ as well as the reduced elements of the electric dipole-moment operator. Its inversion is called the pumping time [6]. The density matrix ρ_g as well as ρ_s implicitly enclose populations of states $\{g\}$ and $\{s\}$, respectively.

The geometrical part of the absorption operator in Eq. (A8) corresponds to the coupling of the jth multipole of the states $\{g\}$ and the lth multipole of the excited light giving a result of rank k.

The multipole moments $\Phi(\mathbf{e})$ of the pumping beam are defined in analogy to those of the emitted light [Eq. (A5)] as the product of the appropriate polarization vectors. Thus, replacing in Eq. (A5) the vectors ϵ by $\mathbf{e}$ and ϵ^* by $\mathbf{e}^*$ one gets the angular momentum coupling diagrams of this new coherency matrix of the laser light.

3. Time evolution of the density matrix

On choosing the direction of the magnetic field as the axis of quantization of the atomic system (z axis), the time evolution of the irreducible components of the density matrix $\rho_s(t)$ due to the simultaneous processes of optical pumping, radiative decay, and atomic collisions in the presence of the constant magnetic field is described by the equations [36]

$$\frac{d}{dt}\rho^k_{s\kappa}(t) = (-\Gamma_k + i\Omega\kappa)\rho^k_{sk}(t) + A^k_\kappa(t) \ , \qquad \text{(A9)}$$

where $\Omega = \mu_B g_J B/\hbar$ is the Larmor precession frequency (μ_B the Bohr magneton and g_J the Landé splitting factor), and Γ_k is the decay rate of the kth multipole moment. For isotropic atomic collisions these decay constants, due to the transformational properties of the state multipoles, are equal for all the $(2k+1)$ components of the kth multipole [37]. Each decay constant can be separated [28] into a part connected with the rate constant Γ for the free radiative decay, which is the same for all multipoles, and a part Γ^{coll}_k accounting for relaxation caused by atomic collisions [28]:

$$\Gamma_k = \Gamma + \Gamma^{\text{coll}}_k \ . \qquad \text{(A10)}$$

The collisional terms are expressed by the cross sections σ_0, σ_1, and σ_2 for depopulation (quenching), disorientation, and disalignment, respectively:

$$\Gamma^{\text{coll}}_k = nv\sigma_k \ . \qquad \text{(A11)}$$

Here n is the number density of atoms and v their mean relative velocity in binary collisions. In our further discussion we neglect the effect of radiation trapping which, however, can be taken into account in a similar way as the collisions [7,8,37].

For simplicity, we make the assumption that prior to the action of the laser pulse ($t < t_0$) all upper levels belonging to $\{s\}$ are not populated and the pumping is weak enough to justify our neglecting of the depopulation of the lower levels as well as effects of saturation and stimulated emission. In the case of a strong or intermediate pumping field one can adopt the results of Hirabayashi *et al.* [31,38]. We also neglect the cascading effect because of the application of selective laser excitation in our experiment. Furthermore, to be able to take advantage of the diagrammatic technique we use the identity [18]

$$\delta_{\kappa'\kappa}\exp[i\kappa\Omega(t-\tau)] = D^k_{\kappa'\kappa}(-\Omega(t-\tau),0,0) \ , \qquad \text{(A12)}$$

where $D^k_{\kappa'\kappa}(R) = D^k_{\kappa'\kappa}(\alpha,\beta,\gamma)$ is the Wigner matrix element [18–20] [Fig. 9(d)] of the rotation R specified by the Euler parameters α, β, and γ. Under these assumptions we obtain the solution of Eq. (A9) in the form

$$\rho^k_{s\kappa}(t) = \int_{t_0}^{t} \exp[-\Gamma_k(t-\tau)]\,\tilde{A}^k_\kappa(t,\tau)\,d\tau \ , \qquad \text{(A13)}$$

where

$$\tilde{A}^k_\kappa(t,\tau) = \sum_{\kappa'} A^k_{\kappa'}(\tau)\, D^k_{\kappa'\kappa}[-\Omega(t-\tau)] = \qquad \text{(A14)}$$

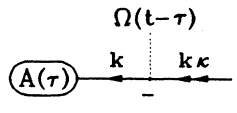

represents the absorption operator $A(\tau)$ in the reference frame rotating around the direction of the static magnetic field **B** with the angular velocity Ω.

4. General geometrical dependence of the fluorescence signal in a static magnetic field

The fluorescence signal is in general not only depending on the geometrical relations between the vectors characterizing the optical $(\epsilon, \epsilon^*, \mathbf{e}, \mathbf{e}^*)$ and magnetic fields $(\mathbf{B})$ but also on the geometrical properties (polarization) of the density matrix ρ_g in the initial Zeeman manifold $\{g\}$. If the atomic beam is prepared by a hollow cathode discharge, self-alignment of the excited states can be obtained [39,40]. However, in the present experiment we neglect this effect because the initial state $\{g\}$ of the neon I state, which is used in the discussion, has zero angular momentum, and thus all multipoles of ranks higher than zero vanish. For such an unpolarized state the geometrical part of the absorption operator in Eq. (A8) due to the properties of the Wigner $3j$ and $9j$ symbols is reduced to the multipole of the pumping light $\Phi(\mathbf{e})$ only. Thus Eq. (A14) now takes the form

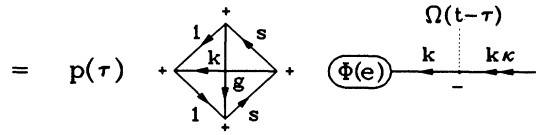

(A15)

Applying the recoupling scheme for Wigner matrices [Figs. 10(h) and 10(i)] we transpose the effect of Larmor precession in Eq. (A15) directly onto the polarization vectors of the laser light:

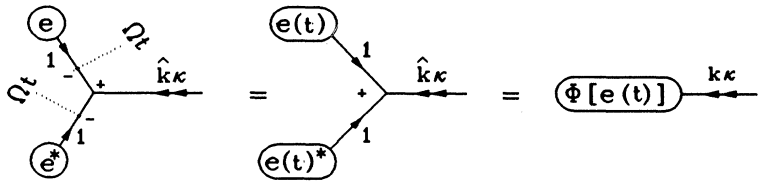

(A16)

The first diagram in Eq. (A16), according to Figs. 10(h) and 10(i) and Eq. (A5), is equal to the geometrical part of the absorption operator in Eq. (A15), while the last one represents the new time-dependent coherency matrix of the pumping laser beam, formed by polarization vectors $\mathbf{e}(t)$ and $\mathbf{e}(t)^*$ of the laser light in the frame rotating with the angular velocity Ω around the vector **B**. Polarization vectors in the laboratory and in the rotating frame are related by [18]

$$\mathbf{e}(t)=\mathbf{e}\cos(\Omega t)+\mathbf{b}(\mathbf{b}\cdot\mathbf{e})[1-\cos(\Omega t)] +(\mathbf{b}\times\mathbf{e})\sin(\Omega t)\ , \tag{A17}$$

where **b** is the unit vector parallel to the magnetic field. This equation, which is independent of the choice of the reference system, causes that our general geometrical relations resulting from Eq. (A17) are also rotationally invariant. Due to the relations (A4), (A5), and (A13)–(A16) the TRLIF signal [Eq. (A1)] takes in presence of a magnetic field the form

$$S(t)=C_S\sum_k \alpha(k)\int_{t_0}^{t} p(\tau)\exp[-\Gamma_k(t-\tau)] \times F_k(t-\tau)d\tau\ , \tag{A18}$$

where C_S contains all time and spatially independent parameters. The anisotropy factor [8,24] $\alpha(k)$ and the general time-dependent geometrical factor $F_k(t)$ is given by

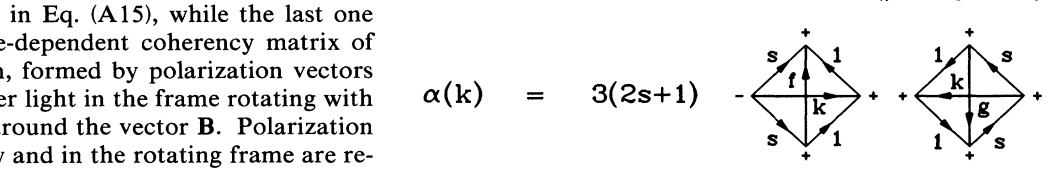

(A19)

and

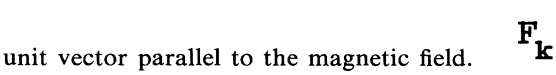

(A20)

respectively. Our Eq. (A19) corresponds to Eq. (3.56) in Ref. [24]. The factor $\alpha(k)$ is normalized to unity for $k=0$. Equation (A18) has a form analogous to the well-known results in the absence of a magnetic field [8], the only difference residing in the replacement of the permanent polarization vector of the excited light by its time-dependent form [Eq. (A17)] in the geometrical part of the TRLIF signal.

To simplify the next steps of our discussion we assume that the duration of the laser pulse is much shorter than

the lifetime of the relevant levels as well as the period of Larmor precession, according to the condition of our experiments. Thus, with a good accuracy, we can treat the function $u(t)$, and consistently $p(t)$, as proportional to the Dirac delta function. Integration in Eq. (A18) now leads immediately to

$$S(t) \propto \sum_k \alpha(k) \exp(-\Gamma_k t) F_k(t) . \quad \text{(A21)}$$

This formula, together with Eqs. (A19) and (A20), provides the geometrical and time characteristic of the TRLIF signal.

[1] W. L. Wiese, J. W. Brault, K. Danzmann, V. Helbig, and M. Kock, Phys. Rev. A **39**, 2461 (1989).

[2] W. L. Wiese, in *The Physics of Ionized Gases*, edited by G. Pichler (The Institute of Physics, Zagreb, Yugoslavia, 1983), p. 435.

[3] W. L. Wiese, J. Quant. Spectrosc. Radiat. Transfer **40**, 421 (1988).

[4] Z. Stryla, H. Pobee, W. Schade, and V. Helbig, Phys. Rev. A **41**, 512 (1990).

[5] J. N. Demas, *Excited State Lifetime Measurements* (Academic, London, 1983).

[6] S. Haroche, in *High-Resolution Laser Spectroscopy*, edited by K. Shimoda (Springer, Berlin, 1976).

[7] J. N. Dodd and G. W. Series, in *Progress in Atomic Spectroscopy*, edited by W. Hanle and H. Kleinpoppen (Plenum, New York, 1978), Pt. A, p. 639.

[8] P. Hannaford and R. M. Lowe, Opt. Eng. **22**, 532 (1983); Austr. J. Phys. **39**, 829 (1986).

[9] H. Figger, K. Siomos, and H. Walther, Z. Phys. **270**, 371 (1974).

[10] M. Gustavsson, H. Lundberg, L. Nilsson, and S. Svanberg, J. Opt. Soc. Am. **69**, 984 (1979).

[11] W. Schade, G. Langhans, and V. Helbig, Phys. Scr. **36**, 890 (1987).

[12] W. Schade, B. Mundt, and V. Helbig, Phys. Rev. A **42**, 1454 (1990).

[13] J. Carlsson, Z. Phys. D **9**, 147 (1988).

[14] T. Fujimoto, C. Goto, and K. Fukuda, Opt. Commun. **40**, 23 (1981).

[15] T. Fujimoto, C. Goto, and K. Fukuda, Phys. Scr. **26**, 443 (1982).

[16] A. P. Jucys (Yutsis), I. B. Levinson, and V. V. Vanagas, *Mathematical Apparatus of the Theory of Angular Momentum* (Israel Program for Scientific Translations, Jerusalem, 1962); A. P. Jucys and A. A. Bandzaitis, *The Theory of Angular Momentum in Quantum Mechanics*, 2nd ed. (Academy of Sciences of the Lithuanian SSR, Institute of Physics, Vilnius, 1977).

[17] I. Lindgren and J. Morrison, *Atomic Many-Body Theory* (Springer, Berlin, 1982).

[18] D. A. Varshalovich, A. N. Moskalev, and V. K. Khersonskii, *Quantum Theory of Angular Momentum* (World Scientific, Chichester, 1987).

[19] E. ElBaz and B. Castel, *Graphical Methods of Spin Algebras in Atomic, Nuclear and Particle Physics* (Dekker, New York, 1972).

[20] D. M. Brink and G. M. Satchler, *Angular Momentum*, 2nd ed. (Oxford University Press, London, 1968).

[21] G. E. Stedman, Adv. Phys. **34**, 513 (1985); C. D. Churcher and G. E. Stedman, J. Phys. C **14**, 2237 (1981).

[22] R. Luypaert and J. Van Craen, J. Phys. B **10**, 3627 (1977).

[23] K. Blum, *Density Matrix Theory and Applications* (Plenum, New York, 1981).

[24] A. Omont, Prog. Quantum. Electron. **5**, 69 (1977).

[25] W. Schade, B. Garbe, and V. Helbig, Appl. Opt. **29**, 3950 (1990).

[26] W. Schade, Laser Optoelektronik **23**, 63 (1991).

[27] W. Schade and V. Helbig, Phys. Lett. A **115**, 39 (1986).

[28] C. G. Carrington and A. Corney, J. Phys. B **4**, 849 (1971).

[29] M. Born and E. Wolf, *Principles of Optics* (Pergamon, Oxford, 1965).

[30] D. W. Duquette, S. Salih, and J. E. Lawler, Phys. Lett. **83A**, 214 (1981).

[31] A. Hirabayashi, S. Okuda, Y. Nambu, and T. Fujimoto, Phys. Rev. A **35**, 639 (1987).

[32] D. W. Duquette and J. E. Lawler, Phys. Rev. A **26**, 330 (1982).

[33] S. Salih, D. W. Duquette, and J. E. Lawler, Phys. Rev. A **27**, 1193 (1983).

[34] J. Carlsson, Z. Phys. D **9**, 147 (1988).

[35] W. Schade and M. Raeth, in *Laser Spectroscopy X*, Proceedings of the 10th International Conference on Laser Spectroscopy, edited by M. Ducloy, E. Giacobino, and G. Camy (World Scientific, Singapore, 1992), p. 414.

[36] M. I. D'yakonov, Zh. Eksp. Teor. Fiz. **47**, 2213 (1964) [Sov. Phys. JETP **20**, 1484 (1965)].

[37] M. I. D'yakonov and V. I. Perel', Zh. Eksp. Teor. Fiz. **47**, 1483 (1964) [Sov. Phys. JETP **20**, 997 (1965)].

[38] A. Hirabayashi, Y. Nambu, and T. Fujimoto, Jpn. J. Appl. Phys. **25**, 1563 (1986).

[39] D. Zhechev, J. Phys. B **18**, 65 (1985).

[40] T. Fujimoto and S. Matsumoto, J. Phys. B **21**, L267 (1988).